



**HAL**  
open science

## A statistical characterisation of the distribution of a cloud of space debris after a break-up in orbit

D. Thomasson, F. Deleflie, A. Petit

► **To cite this version:**

D. Thomasson, F. Deleflie, A. Petit. A statistical characterisation of the distribution of a cloud of space debris after a break-up in orbit. *Acta Astronautica*, 2019, 161, pp.115-124. 10.1016/j.actaastro.2019.04.051 . hal-03151337

**HAL Id: hal-03151337**

**<https://hal.science/hal-03151337>**

Submitted on 25 Oct 2021

**HAL** is a multi-disciplinary open access archive for the deposit and dissemination of scientific research documents, whether they are published or not. The documents may come from teaching and research institutions in France or abroad, or from public or private research centers.

L'archive ouverte pluridisciplinaire **HAL**, est destinée au dépôt et à la diffusion de documents scientifiques de niveau recherche, publiés ou non, émanant des établissements d'enseignement et de recherche français ou étrangers, des laboratoires publics ou privés.



Distributed under a Creative Commons Attribution - NonCommercial 4.0 International License

# A statistical characterisation of the distribution of a cloud of space debris after a break-up in orbit

D. Thomasson<sup>a,\*</sup>, F. Deleflie<sup>b,\*\*</sup>, A. Petit<sup>c,\*\*</sup>

<sup>a</sup>*IMCCE / Observatoire de Paris, PSL Research University, CNRS, Sorbonne Université, Univ. Lille, Impasse de l'Observatoire, 59000 Lille, France*

<sup>b</sup>*IMCCE / Observatoire de Paris, PSL Research University, CNRS, Sorbonne Université, Univ. Lille, 77 Avenue Denfert Rochereau, 75014 Paris, France.*

<sup>c</sup>*IFAC-CNR - Via Madonna del Piano, 10, 50019 Sesto Fiorentino, FI, Italy*

---

## Abstract

This paper aims at proposing a new way of statistically characterising the spatial distribution of a cloud of space debris generated by a fragmentation in orbit, by using a family of functions that is well-known in applied mathematics. Such a family can be very convenient to describe through a few parameters the main features affecting the dynamical evolution of the whole cloud, and the mutual distance between objects within the cloud, at different epochs. The tested population of space debris is supposed to be a configuration of points resulting from the realisation of a point process and what we call “exploratory tools” from spatial statistics are applied to it. The role played by some parameters driving the breakup or the dynamical model on the statistical results is investigated with examples based on Fengyun-1C-like and Molniya-like cases.

*Keywords:*

Space debris, spatial distribution, statistical behaviour, point processes, Fengyun-1C breakup, closure times.

---

## 1. Introduction

The issues related to space debris are now a major concern because their number in orbit has significantly increased during the last years. Space

---

\*Principal corresponding author

\*\*Corresponding author

*Email addresses:* [delphine.thomasson@obspm.fr](mailto:delphine.thomasson@obspm.fr) (D. Thomasson),  
[florent.deleflie@obspm.fr](mailto:florent.deleflie@obspm.fr) (F. Deleflie), [alexis.petit@obspm.fr](mailto:alexis.petit@obspm.fr) (A. Petit)

debris are made up of passive artificial objects in orbit around the Earth, covering a wide range of orbital configurations (semi-major axes, inclinations, eccentricities, ...), and with a huge variety of physical properties (in particular a wide range of Area-to-Mass Ratios (AMR)). Since the launch of Sputnik in 1957, more than 8 000 payloads have been launched in space and more than 4 500 are still in orbit<sup>1</sup> (2018). Intensification of space activities leads to an increasing number of space debris also due to in-orbit fragmentation events. This number is likely to continuously grow in the future in spite of mitigation guidelines recently adopted by working groups such as the Inter-Agency Space Debris Coordination Committee (IADC). Global analyses of the long term evolution of the space debris population are thus still more than expected to investigate the long term sustainability of the space activities.

Two events have particularly contributed in the growth of space debris in low-orbit over the last decade: (i) the destruction of the Fengyun-1C satellite that occurred in 2007 at an altitude of about 860 km and (ii) the accidental collision between Cosmos-2251, a russian inactive telecommunication satellite, and the american active telecommunication satellite Iridium33 that occurred in 2009. This was the first accidental catastrophic collision ever registered between two satellites [1], creating thousands of fragments that spread out between 200 and 4 000 km in altitude. These two catastrophic events are at the origin of a wide literature, dealing with their consequences on the long term evolution of space debris in the Low-Earth-Orbit (LEO) region ([1, 2, 3, 4, 5, 6, 7]).

In this framework, this paper aims at proposing a new way of statistically characterising the spatial distribution - in view of collision risk evaluation - of a cloud of space debris generated by a fragmentation in orbit, by using a family of functions that is well-known in applied mathematics, and that we find very convenient to be used in the framework of space debris. We are particularly interested in the short term evolution of the cloud as the fastest changes in the spatial distribution occur during the first revolutions after the fragmentation. Section 2 introduces statistical tools adapted to space debris issues while Section 3 describes the dynamical model to carry out the simulations. In Section 4, the role played by some parameters driving the breakup or the dynamical model on the statistical results is investigated with an example based on a Fengyun-1C-like case ; finally conclusions and

---

<sup>1</sup>According to Centre National d'Études Spatiales (CNES) website (<https://debris-spatiaux.cnes.fr/>) and Space-track reports (<https://www.space-track.org/>)

prospects are highlighted in Section 5.

## 2. *G*-function: a tool to statistically characterise the spatial properties of a cloud of debris

The concentration of objects within a cloud of space debris can be enhanced by statistical tools such as what is called “exploratory statistics”. We base the rest of the paper on such a function, called *G*, that we define hereafter.

The space debris population (or parts of it) is described as being a realisation of a point process *X* that stands for a mathematical model describing random configurations of points. This is a mathematical object more than well-known by mathematicians but that we recall here to be self-consistent. The points configurations are observed in an observation window denoted *W*, that can be here a torus around the parent body’s orbit. The intensity  $\lambda$  of such a point process corresponds to the mean number of points per volum unit (independently from their mass). To adapt the usual formalism to space debris populations, the following hypotheses are added: (i) the tested population of space debris is supposed to be a configuration of points resulting from the realisation of a point process (that is not that obvious), (ii) the point process is considered to be locally stationary, implying that a translation of the point configuration will not change its statistical properties. In other words, the results of the computation will not depend on how the observation window is defined and  $\lambda$  will be the same everywhere in *W* that can be defined as the convex envelope of the cloud:

$$\lambda = \lambda_0 = \frac{\mathbb{E}N(X)}{\nu(W)}. \quad (1)$$

with  $\mathbb{E}N(X)$  the mathematical expectation of the point process *X* number of points (that corresponds to the mean number of points, that is then fixed once for all), and  $\nu(W)$  the volum of the observation window *W*.

In practice, informations on the model to be built are obtained by carrying out an *exploratory analysis* that defines how summary characteristics can give hints on the behaviour of the point process. These characteristics are based on the computation of the moments of the distribution. In the following, we use the “nearest-neighbour distance distribution function” *G*(*r*) [8]: let *b*(*x*,*r*) be a ball or radius *r* > 0 centred in *x*, a point of the point process *X*, and let  $\rho(x, X)$  be the minimum Euclidean distance between *x*

and another point of  $X$ . The  $G$ -function describes the probability of finding a point of  $X$  in that ball without counting  $x$  itself,

$$G(r) = \mathbb{P}_x(\rho(x, X \setminus \{x\}) \leq r). \quad (2)$$

The way the  $G(r)$  function is estimated has to be carefully defined : interactions are possible between points that lie outside the observation window (and for which we have no information) and points of the point process located near the border of  $W$ , as an *edge effect* [9]. In order to overcome this problem, we consider only the points which are located at a minimal distance from the border. This method is the one used to construct the *Border Method estimator* [10, 11, 12, 13]:

Let  $X$  be a stationary point process, and  $W$  its observation window.  $\rho(x, X \setminus \{x\})$  and  $\rho(x, \partial W)$  are the minimum Euclidean distance between a point of the process and (i) its nearest neighbour, and (ii) the border of the window  $\partial W$ , respectively, we have [9]:

$$\hat{G}(r) = \frac{\sum_{x \in X} \mathbb{1}\{\rho(x, X \setminus \{x\}) \leq r\} \cdot \mathbb{1}\{\rho(x, \partial W) > r\}}{\sum_{x \in X} \mathbb{1}\{\rho(x, \partial W) > r\}}. \quad (3)$$

where  $\mathbb{1}(\cdot)$  is the indicator function defined as follows:

$$\mathbb{1}(x \in X) = \begin{cases} 1 & \text{if } x \in X \\ 0 & \text{otherwise} \end{cases}. \quad (4)$$

**Figure 1 illustrates the estimation of the  $G$ -function for a point process in two dimensions at a fixed time ; the idea is exactly the same in 3D. The black crosses correspond to the points  $x$  of the point process studied  $X$  defined in the observation window  $W$  depicted by the black rectangle. In a space debris point of view, the crosses stand for the fragments generated by an on-orbit breakup and the whole cloud of objects can be seen as the point process. In order to estimate the  $G$ -function, we center a circle (or ball in 3D) of radius  $r$  on one of the crosses ; this is represented by the blue cross and circle on Figure 1. Then, we count the number of other points (i.e.: other crosses) that are located inside the blue circle and at a distance greater than  $r$  of the window boundary. This last condition, to determine which crosses have to be considered for the estimation, comes from our choice to use the border method estimator. After, the center of the**

circle is changed and becomes one of the remaining points, until all the points of the point process have been selected. The result is finally normalised by the total number of points belonging to the point process that is equivalent to the total number of fragments belonging to the generated cloud. This process is repeated for other values of the circle's radius  $r$  to get the  $G$ -function estimation for several neighbourhoods at a fixed time.

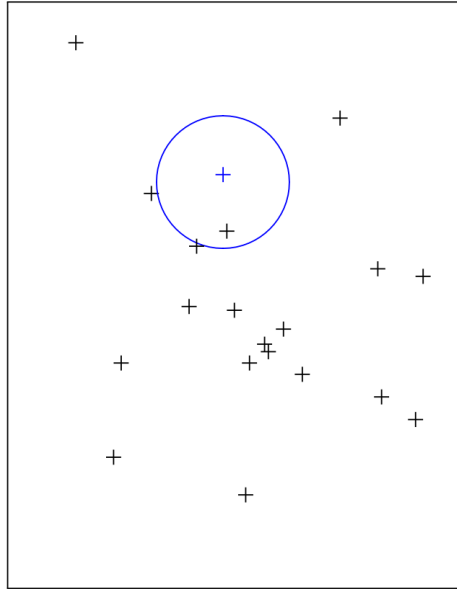


Figure 1: Graphical illustration of the estimation process of the  $G$ -function by using the border method estimator for a point process in two dimension. The black crosses correspond to the points  $x$  of the point process studied  $X$  defined in the observation window  $W$  depicted by the black rectangle.

In the following sections, to investigate the role played by the parameters in the model - such as the typical (maximum) velocity increment value and the position and orbit characteristics of the parent satellite -, the  $G$ -function estimation evolution is plotted with respect to time for a fixed radius. The estimation is always based on Equation (3) ; but picking the value of the probability for a given radius and for each epoch, provides a view of the temporal evolution of the estimation. Let us note that it is not a formal estimation of the  $G$ -function with respect to time, but only a change of the plotted variables: instead of plotting the estimation of the  $G$ -function with respect to the radius of the ball for a fixed time, we choose a radius and

pick the results of the estimation for different epochs to get the graphical representation. The selection of radii is based on the corresponding “time distance” between objects within the cloud. For example, if the radius chosen is equal to 100 km and the relative velocity of the objects is 10 km/s, the corresponding time distance is of the order of 10 seconds. That is, the  $G$ -function provides the probability of finding a neighbour 10 seconds away from a piece of space debris within the observation window that is chosen.

### 3. Modeling

#### 3.1. Breakup Model

In this paper, as we are interested in the first place in the study of the impact of some parameters changes (velocity increment distribution, initial conditions of the parent body), a simplified model that determines only the velocity increment distribution is convenient. Moreover, as we are not interested in the consequences of the choice of the statistical law used to derive the  $\Delta V$  distribution, only the influence of the parameters related to one particular statistical law are studied. **In this framework, the breakup model used for the simulation is based on a uniform law applied to each of the three directions defining the local frame with minimum and maximum boundaries for the velocity increment distribution. These boundaries are set symmetric to zero (as the event is considered as isotropic), and defined by a percentage  $p$  applied to the parent satellite velocity at the epoch of the event. The uniform distributions are then used in the local frame of the parent body to generate the initial conditions of each fragment created by the breakup. The number of generated objects being invariant and set equal to 500 (arbitrarily) for all the simulations throughout this paper, the only parameter that is modified in the different test cases is the value of the percentage to be applied. Finally, the  $\Delta V$  distribution law for our simplified breakup model is defined by Equation (5).**

$$D_{\Delta V}^{simple}(\mathbf{max}) = \mathcal{U}(\mathbf{max}, -\mathbf{max}) \quad (5)$$

where  $\mathbf{max} = p\% \times V_{sat}$  with  $p \in \mathbb{R}$ .

To consider more parameters, such as the number of fragments, the size or Area-to-mass (A/m) ratio distributions, the NASA Breakup Model could be used in a future study.

### 3.2. Dynamical Model

The propagation is performed with the “FAST” software (Finalised Analytical Satellite Theory © CNES/IMCCE). The approach used in this software for the orbital modeling is based on an analytical theory to get orbital element time series [14]. **An analytical method, instead of numerical, avoids important computation times and the model is accurate enough to be considered as representative of the main features affecting both the cloud and single objects: changes of the orbital period (due to a change of the semi-major axis), and the secular variations of the right ascension of ascending node and of the argument of perigee. It is then relevant to consider only the perturbations due to the geopotential up to  $J_2$  (first order). Indeed, as we look for the effect of a change of velocity of the order of a few percent, roughly speaking only the  $J_2$  parameter is significant. As it can be established from the integral of energy that  $\Delta a = \frac{2}{n} \Delta V$ , and since  $n$  is of the order of  $10^{-3} \text{ rad.s}^{-1}$ , only the perturbations inducing changes of the semi-major axis greater than 2 km, namely  $J_2$ , have to be taken into account.**

In order to consider all the values of eccentricity or inclination (small or large), the model is written in a set of equinoctial elements  $\mathbf{E}$  composed by a mean part  $\bar{\mathbf{E}}$  and a short periodic part  $\Delta\mathbf{E}$ , so as to write:

$$\mathbf{E}(t) = \bar{\mathbf{E}}(t) + \Delta\mathbf{E}(t)$$

The mean part  $\bar{\mathbf{E}}$  is governed by the secular variations induced on angular elements by the dynamical flattening of the Earth  $J_2$ :

$$\begin{aligned}\dot{\Omega} &= -\frac{3}{2} \left( \frac{R_e}{a} \right)^2 \bar{n} J_2 \frac{\cos i}{(1-e^2)^2} \\ \dot{\omega} &= -\frac{3}{4} \left( \frac{R_e}{a} \right)^2 \bar{n} J_2 \frac{1-5\cos^2 i}{(1-e^2)^2}, \\ \dot{M} &= \frac{3}{4} \left( \frac{R_e}{a} \right)^2 \bar{n} J_2 \frac{1-3\cos^2 i}{(1-e^2)^{3/2}}\end{aligned}$$

The short periodic part  $\Delta\mathbf{E}$ , read  $\Delta\mathbf{E} = \mathcal{L}(\bar{\mathbf{E}}) \frac{\partial W_{gen}}{\partial \bar{\mathbf{E}}}$ , is governed by the Lagrange Planetary Equations written in a  $6 \times 6$  matrix  $\mathcal{L}(\bar{\mathbf{E}})$  and by a generating function  $W_{gen}$  dealing with the short periodic part of the motion. In this paper, it is convenient to only account for the short periods induced

by  $J_2$ , as we work mainly in LEO meaning that the order of the short periods maximum amplitude due to  $J_2$  is 10 km while the order of the most important other short periods (due to other orbital perturbations) is the kilometer at most.

On another hand, knowing that the  $\Delta V$  applied to the parent satellite to generate the breakup is very small with respect to the velocity of the parent body (order of  $\text{m.s}^{-1}$  and  $\text{km.s}^{-1}$  respectively) and that the short periods induced by  $J_2$  are of first order, this implies that the addition of the short periodic terms is completely negligible when the velocity increments are applied (in the local frame). It can be verified with the equations developed by [15] presenting, in the local frame, the velocity variations generated by the geopotential derived from Kaula's equations that describe the satellite motion into the gravitational field of a rigid body. In the tangential direction we have:

$$\Delta v_\tau = na\Delta e \sum_{s=1}^{\infty} sN_s \cos sM - n\Delta a \sum_{s=0}^{\infty} \frac{1}{2}K_s \cos sM - na(\Delta\omega + \Delta\Omega \cos i) \sum_{s=1}^{\infty} sH_s \sin sM \quad (6)$$

where,

$$\begin{aligned} N_s(e) &= \frac{2}{se\sqrt{1-e^2}} J_s(se) \\ K_s(e) &= (2 - \delta_{0s})\sqrt{1-e^2} J_s(se) \\ H_s &= -\frac{2e}{s^2} J'_s(se) \end{aligned}$$

with  $J_s(se) = \sum_{p=0}^{\infty} \frac{(-1)^p}{p!(s+p)!} \left(\frac{se}{2}\right)^{2p+s}$  the Bessel function of first kind.

By considering Equation (6) up to the first order and small eccentricities, and by converting the variations in  $\omega$ ,  $\Omega$  and  $e$  ( $\Delta\omega$ ,  $\Delta\Omega$  and  $\Delta e$  respectively) in term of  $\Delta a$  so as to get  $\Delta e = \Delta\omega = \Delta\Omega = \frac{\Delta a}{a}$ , some simplifications are made.

$$\Delta v_\tau \approx 2n\Delta a - n\Delta a + 2ne(\Delta a + \Delta a \cos i) = (n + 2ne(1 + \cos i)) \Delta a$$

The main term of this last equation is the quantity  $n\Delta a$  which is of  $10 \text{ m.s}^{-1}$  order. Similar results are obtained for radial and out-of-plan directions. Then, the change of velocity at the event epoch

**can be applied either to the mean or osculating elements (they have the same orders of magnitude) and they are then transformed into a position/velocity vector by applying usual transformations.**

### *3.3. Spatial evolution of a space debris cloud*

As described by [16] or [17], four different phases can be considered after a break-up of a satellite in orbit. During the first phase (Phase A) that lasts only a couple of hours, the cloud can be represented as a “pulsating ellipsoid”. But quickly - a few hours after the breakup in LEO -, the semi-major axis differences between the created objects leading to different orbital periods, the ensemble spreads along the parent’s body orbit and forms a torus (Phase B). Then, due to the non-sphericity of the Earth, the torus opens to a band limited in latitude by the inclination of the parent satellite (Phase C). The transition between Phase B and C can take several years as  $\Omega$  and  $\omega$  have a period of the order of years. The last phase (Phase D) starts right after the complete nodal and apsidal dispersion. Until the beginning of Phase D, it can be considered that the motion of the fragments is mainly perturbed by the geopotential. It is only during the last phase that the perturbation due to the atmospheric drag becomes dominant and the orbital decay begins.

In this paper, we focus in particular on the evolution of the fragments during the Phase B (i.e. torus formation) that is a quick step in the spatial evolution process of the cloud. Moreover, as the main perturbation of the motion during this phase is due to the geopotential, this is the only one considered for the orbit propagation/dynamical modeling.

## **4. Statistical analysis of the apsidal closure time (short term)**

In this section, the fragmentation of a Fengyun-1C-like orbit is investigated: an orbit in the LEO regime ( $a \approx 7228$  km), almost circular ( $e \approx 0.00135$ ) with an inclination of about  $98^\circ$  and a keplerian orbital period of approximately 1 hour and 42 minutes, that makes the simulation be very close to a Sun-synchronous configuration. Breakup simulation is performed with the simplified breakup model (Section 3.1) while the orbit propagation is carried out with the software described in Section 3.2. We study the consequences of the choices of the following model parameters as revealed by statistical functions defined above: **magnitude of the ejection velocity of the fragments**, parent body’s orbit characteristics and position along the orbit where the breakup occurs.

#### *4.1. Influence of the choice of the maximum change of velocity allowed by the breakup model*

A set of  $\Delta V$ , with norm and orientation randomly distributed in space, is applied to the velocity vector of the parent body. **Based on the positions and velocities of the real observed fragments in April 2008 and on the velocity of the parent body, derived from the initial conditions, the velocity increments distribution of the generated fragments is determined.** The datafile containing the positions and velocities of the fragments at the reference epoch 04/23/2008 has been provided by Carmen Pardini and Luciano Anselmo and is described in [3]. From the study of this  $\Delta V$  distribution, and in particular by the examination of the data serie quantiles, it can be established that approximately 99% of the objects have a  $\Delta V$  of about 435.6 m/s or less with respect to the parent body’s velocity. We then notice that by choosing 6% as the maximum percentage of the parent satellite velocity at the epoch of the event, we get 444 m/s as the maximum value for the velocity increment that is close to the previous value derived from the provided datafiles. Then, for the first case that will be called “realistic” hereafter, in particular in term of distribution, the maximum value of the  $\Delta V$  distribution is set equal to 6% of the parent body velocity. For the other test cases, we chose two values of percentage to get a “low” case with a maximum value of 1% of the parent satellite velocity and a “high” case with a maximum value of 9%. For the three cases, the breakup is considered as isotropic (500 fragments generated) and the initial conditions of the propagation over two days are the last Two-Line-Elements (TLE) known before the Fengyun-1C satellite breakup. The perturbations considered are only those due to the  $J_2$  term of the geopotential.

Figure 2 shows the shape of the cloud for the “low” and “realistic” cases (left and right respectively). This figure figures out the influence of  $\Delta V$  changes in the shape of the torus, meaning that the geometric properties of the generated torus characterise the strength of an in-orbit fragmentation event. Minimum and maximum variations in inclination and perigee/apogee positions are summarised in Table 1.

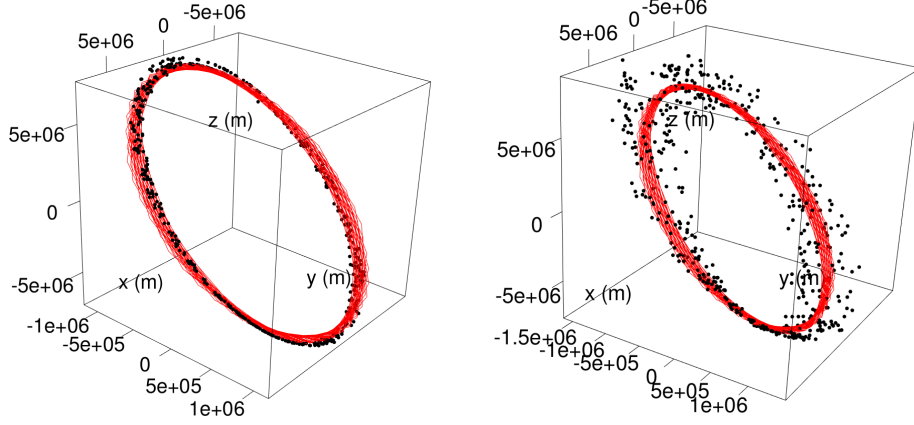


Figure 2: Left: shape of the cloud for the “low” fragmentation case. Right: shape of the cloud for the “realistic” fragmentation case. In both cases, the epoch chosen corresponds to 2 days after the breakup and the red orbit represents the evolution of the parent satellite during the simulation if the breakup does not occur (we can notice the effect of the node’s secular drift). Moreover, it seems from the naked eye that we are over the apsidal closure time, as the torus is already completed.

Table 1: Minimum and maximum variations in perigee/apogee positions (in kilometers) and inclination (in degrees) induced by the fragmentation event. The maximum value of the  $\Delta V$  applied to the parent body leads to major changes in the geometry of the torus generated, giving hints on the strength of the breakup event.

	Min. $r_p$ (km)	Max. $r_a$ (km)	Min. $\Delta i$ (deg)	Max. $\Delta i$ (deg)
Max. $\Delta V = 1\%$	7 220.712	7 653.313	$1.29 \times 10^{-4}$	0.61
Max. $\Delta V = 6\%$	7 220.710	10 287.262	$8.10 \times 10^{-4}$	3.57

Figures 3, 4 and 5 show the evolution of the probability of finding a neighbour with time for different radii (namely 70 km, 140 km and 210 km) and for the three  $\Delta V$  cases. The radii are chosen based on the time distance they correspond to: the time distance for a velocity of the order of  $7 \text{ km}\cdot\text{s}^{-1}$  and a radius of 70 km is equal to 10 seconds (respectively 20 seconds and 30 seconds for radii of 140 km and 210 km). Therefore, on Figure 3 the fragments are approximately and not greater than 10 seconds (respectively 20 seconds and 30 seconds) distant from each other corresponding to a space radius of 70 km (respectively 140 km and 210 km). Any other practical conversion factor between space and time would have been convenient as well to enlighten the main features affecting the evolution of the probability. The time distance values are determined from the velocity of the parent

body and are based on the assumption that this velocity is approximately equal to  $7 \text{ km.s}^{-1}$ . **As the generated fragments do not have the same velocities within the cloud, the selected time distance can be seen as an approximation that corresponds to the truth, but only for an averaged point of view.**

**The obtained probabilities are plotted with a logarithmic scale. Their estimation is carried out every 10 minutes over a period of 2 days (propagation time of the orbits).**

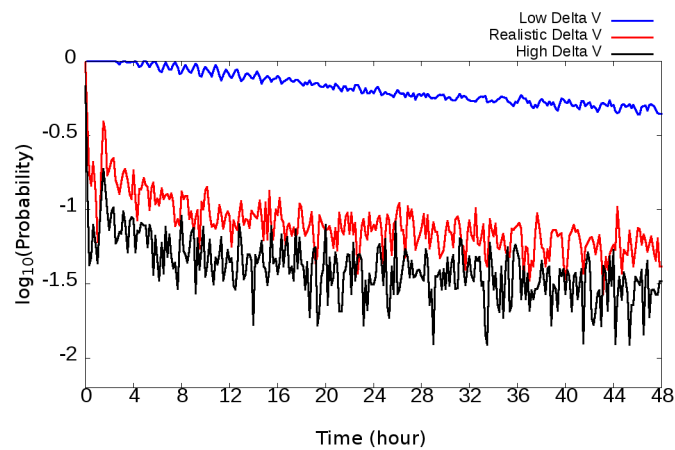


Figure 3: Probability of finding a neighbour ( $G$ -function) in a radius of 70 km from a space debris after the simulation of fragmentation. The blue curve stands for the “low” case, the red one represents the “realistic” case and the black curve corresponds to the “high” case. The estimation of the  $G$ -function is carried out every 10 minutes over a period of 2 days.

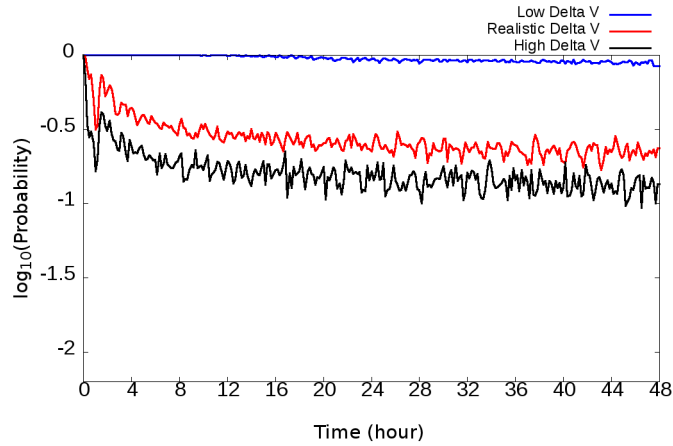


Figure 4: Probability of finding a neighbour ( $G$ -function) in a radius of 140 km from a space debris after the simulation of fragmentation. The blue curve stands for the “low” case, the red one represents the “realistic” case and the black curve corresponds to the “high” case. The estimation of the  $G$ -function is carried out every 10 minutes over a period of 2 days.

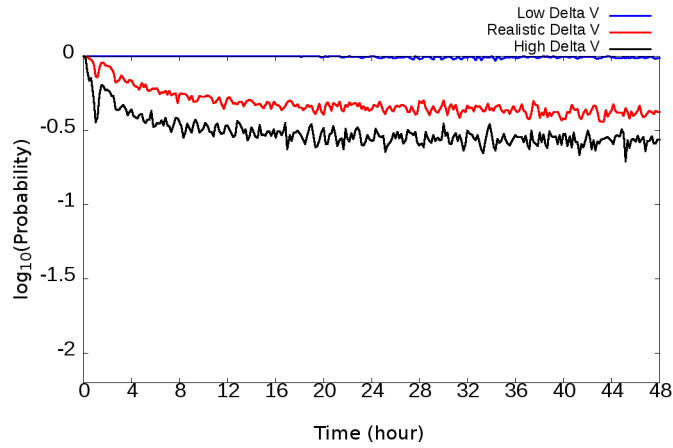


Figure 5: Probability of finding a neighbour ( $G$ -function) in a radius of 210 km from a space debris after the simulation of fragmentation. The blue curve stands for the “low” case, the red one represents the “realistic” case and the black curve corresponds to the “high” case. The estimation of the  $G$ -function is carried out every 10 minutes over a period of 2 days.

The probability inside the cloud varies a lot with time, especially during the first revolutions around the Earth after the fragmentation. This is due to the short distance between objects within the cloud, distance that

evolves with time along the orbit, because of the differences in orbital period for each created fragment. Indeed, the maximum mean motion change relative to the parent satellite is approximately equal to  $2.56 \times 10^{-4} \text{ rad.s}^{-1}$  and leads to a maximum variation in orbital period of about 34 minutes after the fragmentation, which is a lot, relative to the parent body's period ( $\approx 100$  minutes).

For the “low” case when the radii selected are 140 km and 210 km, the oscillations, although present, are less visible during the first revolutions after the breakup. This is explained by the fact that the strength of the event is not important enough to spread all the fragments during the first revolutions, so all the debris can be found in a neighbourhood of 140 km and thus obviously in a 210 km neighbourhood, at least during the first hours of the simulation.

Nevertheless, for all the test cases and all the radii considered, the global tendency is the decrease of the probability with time as the cloud spreads along the parent satellite orbit. As expected, the probability value is always bigger in a radius of 210 km around a space debris than for other radii, even at the end of the propagation. Moreover, and as expected as well based on the cloud shapes displayed on Figure 2, the probability of finding a neighbour within a given perimeter, defined by the ball radius  $r$  decreases with the increase of the maximum value of the  $\Delta V$  applied, corresponding to a more important spatial distribution of the objects.

The  $G$ -function tends to stabilise through time for all the radii based on Figures 3 to 5 but the simulation is only performed over 2 days. When the simulation duration is pushed to 10 years, for all the study cases, this tendency is confirmed: for the “realistic” case (**maximum  $\Delta V$  set equal to 6% of the parent satellite velocity**), the probability of finding a neighbour tends to 0 for a radius of 70 km and to  $1 \times 10^{-3}$  for radii of 140 km and 210 km. These results lead to the observation that the distribution of the cloud tends to the uniformisation through time ; as the probability of finding a neighbour does not evolve anymore, the minimum distance (mean euclidean) between the fragments tends to become constant.

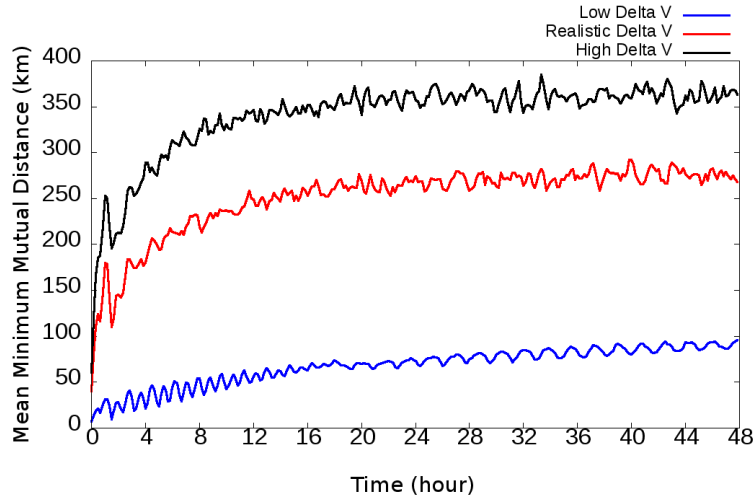


Figure 6: Evolution of the mean minimum euclidean distance between the cloud fragments through time, after the simulation of the breakup. The blue curve stands for the “low” case, the red one represents the “realistic” case and the black curve corresponds to the “high” case. For the three cases, this distance tends to stabilise with time.

#### 4.2. Influence of the orbit characteristics on the $G$ -function

This section aims to give a general overview of the properties provided by the  $G$ -function depending upon the kind of dynamical family of the objects that may be affected by a breakup or a collision. Four kinds of orbits are compared:

- the Fengyun-1C type used previously,
- an Iridium-like orbit (differences in inclination and semi-major axis),
- a geostationary type (the one of a telecommunication satellite belonging to the BSAT family),
- a Molniya type (high eccentricity and inclination quite close to the critical inclination).

To simulate the evolution of a satellite on these orbits, the TLE of four existing space systems are chosen. First, the last TLE of the chinese satellite Fengyun-1C before its breakup, then the recent TLE’s of the payload Iridium-125 (reference epoch: 10/12/17), of the japanese satellite BSAT-4A (reference epoch: 10/17/17), and finally of **the satellite Molniya 3-50**

(reference epoch: 10/17/17) are used. **The orbital elements deduced from the TLE of these four parent bodies are summarised in Table 2.**

A fragmentation generating 500 pieces of space debris is parameterised in order to correspond, for all the test cases, to the “realistic” case described before. For Iridium and Fengyun systems, the maximum velocity increment applied is equal to 6% of their velocity at the event epoch, in order to get a maximum value of  $444 \text{ m.s}^{-1}$  (as the initial velocity is approximately equal to  $7 \text{ km.s}^{-1}$ ). **The Molniya parent body being located close to the orbit’s perigee at the epoch of the event ( $M = 15^\circ$ ), its velocity is of the order of  $6 \text{ km.s}^{-1}$  and concerning the BSAT satellite, its velocity at the epoch of the selected TLE is equal to  $3 \text{ km.s}^{-1}$ . Then, in order to generate breakups with equivalent strengths, the percentages applied to the parent bodies Molniya and BSAT are changed to produce a maximum  $\Delta V$  of about  $450 \text{ m.s}^{-1}$  corresponding to the realistic study case. We chose 15% and 7% of the parent satellites velocities BSAT and Molniya respectively at the epoch of the fragmentation (depending on the TLE) to define the maximum boundary of the  $\Delta V$  distribution for these two systems. The orbit propagation of the generated fragments, for all the study cases, is performed over 2 days considering the long periods of the geopotential term (up to  $J_2$ ) as the only perturbation, namely secular variations on the angles. The consideration of the  $J_2$  term only may not be sufficient to properly reproduce the cloud evolution of Molniya and GEO orbits as they are located deeper in space than Iridium or Fengyun ones. Nevertheless, the main purpose of the study here is not the dynamics, but focus on investigating the effect of orbit characteristics on a spatial statistic such as the  $G$ -function. A more complete examination should nonetheless be carried out, considering in particular (beyond the atmospheric drag for low orbits) the luni-solar perturbations and the Solar radiation pressure to go further in the analysis for GEO and Molniya orbits.**

Figure 7 shows the results obtained for the  $G$ -function time dependency from the epoch of the fragmentation in a radius of 70 km and 210 km for the Fengyun-1C study case. **The curves are the same as the red ones on Figure 3 and 5. They are reproduced here on the same plot, with a logarithmic scale for the probability (Fengyun and Iridium cases) in order to allow a better comparison between all the generated clouds.** Figures 8, 9 and 10 present the probability evolution with time for

Table 2: Orbital elements used as initial conditions of the breakup simulations on Fengyun-1C, Iridium, geostationary and Molniya types of orbits with :  $a$  the semi-major axis (in km),  $e$  the eccentricity,  $i$  the inclination (in degrees),  $\Omega$  the right ascension of ascending node (in degrees),  $\omega$  the argument of perigee (in degrees) and  $M$  the mean anomaly (in degrees). They are deduced from the last known TLE before the simulation of the explosion.

Reference epoch	Satellite	$a$ (km)	$e$	$i$ (deg)	$\Omega$ (deg)	$\omega$ (deg)	$M$ (deg)
01/08/2007	Fengyun-1C	7 228.4508	0.00135	98.6462	0.784894	269.9602	90.00278
10/12/2017	Iridium-125	6 992.8238	0.00118	86.6819	270.6352	216.056	231.8937
10/17/2017	BSAT-4A	42 166.44	0.00032	0.0334	315.0733	178.6097	336.2083
10/17/2017	Molniya 3-50	26 555.82	0.7224	62.1119	229.9198	267.7421	15.9127

Iridium, geostationary and Molniya cases respectively. **The usual scale (bounded between 0 and 1) is preferred to the logarithmic scale for geostationary and Molniya test cases in order to avoid a loss of informations on the  $G$ -function variations due to the important number of null values obtained for the estimation.**

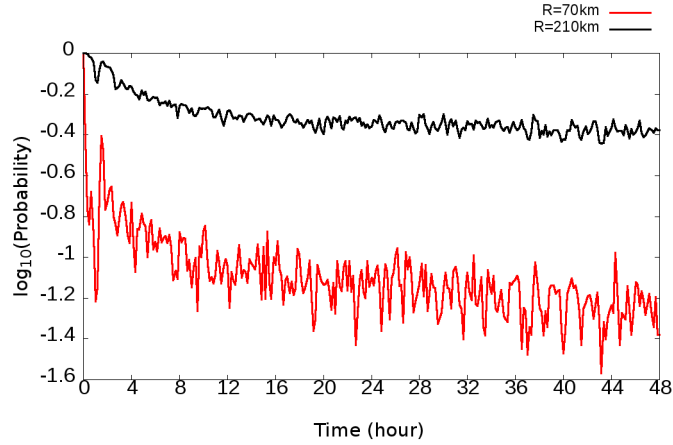


Figure 7: Probability of finding a neighbour in a given radius from a space debris after the simulation of fragmentation for a Fengyun-1C-like type of orbit at the reference epoch 01/08/2007. Initial conditions are set as follows:  $a = 7\,228.4508$  km,  $e = 0.00135$ ,  $i = 98.6462^\circ$ ,  $\Omega = 0.784894^\circ$ ,  $\omega = 269.9602^\circ$  and  $M = 90.00278^\circ$ . The red curve corresponds to a radius of 70 km while the black one stands for a radius of 210 km.

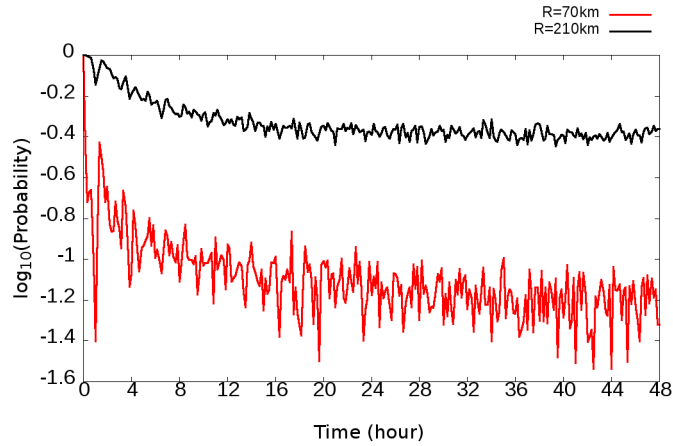


Figure 8: Probability of finding a neighbour in a given radius from a space debris after the simulation of fragmentation for an Iridium-like orbit at the reference epoch 10/12/17. Initial conditions are set as follows:  $a = 6992.8238$  km,  $e = 0.00118$ ,  $i = 86.6819^\circ$ ,  $\Omega = 270.6352^\circ$ ,  $\omega = 216.056^\circ$  and  $M = 231.8937^\circ$ . The red curve corresponds to a radius of 70 km while the black one stands for a radius of 210 km.

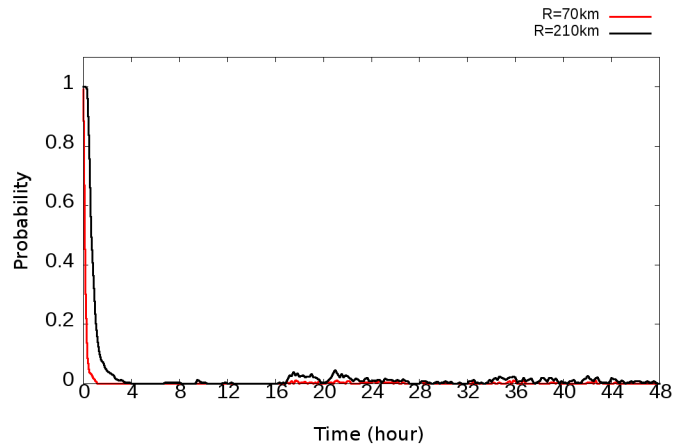


Figure 9: Probability of finding a neighbour in a given radius from a space debris after the simulation of fragmentation for a geostationary type of orbit at the reference epoch 10/17/17. Initial conditions are set as follows:  $a = 42166.44$  km,  $e = 0.00032$ ,  $i = 0.0334^\circ$ ,  $\Omega = 315.0733^\circ$ ,  $\omega = 178.6097^\circ$  and  $M = 336.2083^\circ$ . The red curve corresponds to a radius of 70 km while the black one stands for a radius of 210 km.

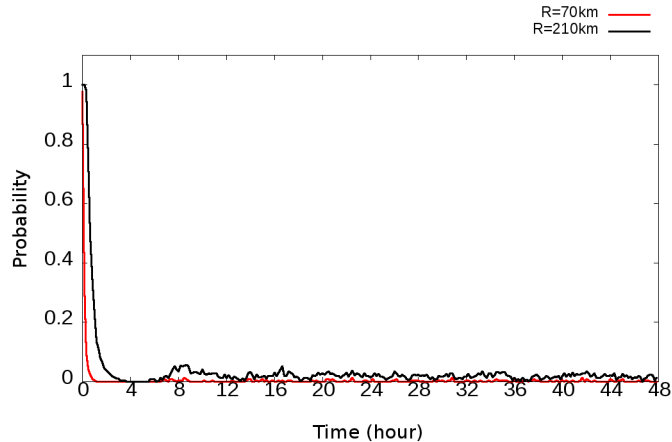


Figure 10: Probability of finding a neighbour in a given radius from a space debris after the simulation of fragmentation for a Molniya-like type of orbit at the reference epoch 10/17/17. Initial conditions are set as follows:  $a = 26\,555.82$  km,  $e = 0.7224$ ,  $i = 62.1119^\circ$ ,  $\Omega = 229.9198^\circ$ ,  $\omega = 267.7421^\circ$  and  $M = 15.9127^\circ$ . The red curve corresponds to a radius of 70 km while the black one stands for a radius of 210 km.

The results obtained with this approach for the cases Iridium and Fengyun are almost the same because these Low-Earth-Orbits have similar characteristics and in particular, they present a very low eccentricity and an inclination between  $85^\circ$  and  $100^\circ$  ( $86.7^\circ$  for Iridium and  $98.6^\circ$  for Fengyun). The behaviour of the  $G$ -function may then be the same for quasi-circular orbits but with a dependence on the number of fragments generated by the fragmentation. Indeed, here, the same supposed number of space debris is created for the four cases, but the decrease (respectively increase) of this number will lead to a decrease (respectively increase) of the probability of finding a neighbour in a given radius.

**For the Molniya case, the probability of finding a neighbour in a radius of 70 km and 210 km quickly tends to 0 ( $1.6 \times 10^{-3}$  and  $1.5 \times 10^{-2}$  respectively on average for the last 10 epochs) based on Figure 10. The velocity differences along the trajectory tend to spread the space debris cloud and only a little bit more than a revolution (12h) is necessary to stabilise the probability, meaning that the parent satellite orbit is populated.**

**These observations are illustrated by Figure 11 with: on the left the shape of the cloud 8 hours after the explosion and on the right this same cloud 16 hours after the event.**

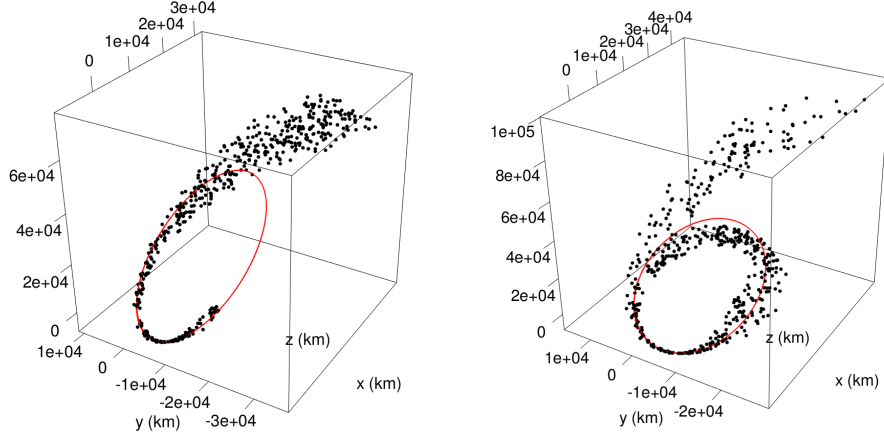


Figure 11: 3D representation of the Molniya cloud. Left: shape of the cloud 8 hours after the explosion. Right: shape of the space debris cloud 16 hours after the explosion. In both cases, the red orbit stands for the evolution of the parent satellite during the simulation if the breakup does not occur. A little bit more than 12 hours are necessary to spread all the fragments along the parent body's orbit.

Finally, for the geostationary-like orbit, the probability of finding another fragment in a neighbourhood of 70 km around a piece of space debris is equal to zero at the end of the simulation. The same observation is made for a radius equal to 210 km, even if in that case the mean value of the probability is equal to 0.00492 for the last ten propagation epochs. **Techniques based on the  $G$ -function lead to very small or null probabilities to detect a fragment in a radius of 210 km, but a slight increase is visible between about 16 hours and 27 hours and then from 33 hours at least after the occurrence of the explosion. Two arguments, based on eccentricity and orbital period, can explain these variations.**

On one hand, at the end of the propagation, the mean value of the fragments' eccentricity is approximately equal to 0.175, with a maximum value of 0.413. Knowing that the initial eccentricity of the parent body is approximately equal to  $3 \times 10^{-4}$  (almost zero) at the reference epoch, the objects generated by the fragmentation have an eccentricity three orders greater than the initial one on average, indicating a more important spreading of the cloud elements. This observation also means that differences between apogee and perigee radius may become significant over time.

On the other hand, it is interesting to determine the orbital pe-

riods of the fragments, as some of them can be different from 24 hours. These deviations in orbital period, with respect to the one (usual) of a geostationary satellite, can influence the spatial distribution of the space debris cloud. The calculations show that the minimum orbital period is around 16 h 20 min, explaining the start of the probability increase, and the maximum value is approximately equal to 51 h 53 min. Moreover, the orbital period of approximately 60% of the fragments is less than 27 hours, explaining the (small) decrease between 27 hours and 33 hours. From that moment, the estimations slowly begin to increase again because the space debris that have already realised one revolution are located in the neighbourhood of the ones presenting an orbital period of 33 hours or more. After that, the probability of finding a neighbour stabilises, indicating that the environment of the parent body trajectory is populated (not necessarily uniformly). These remarks can be verified graphically with the representation in three dimensions of the space debris cloud generated by the fragmentation of a system evolving on a geostationary orbit on Figure 12. On top left, the cloud is plotted 12 hours after the explosion in order to visualise its shape before the first increase of the probability around 16 hours after the event ; the spreading of the fragments is already important and clearly visible. Then, on top right, the shape of the cloud is presented 27 hours after the explosion (top view) ; the differences in orbital period of the fragments relative to the parent body can be clearly distinguished. Finally, at the bottom, the shape of the cloud is plotted 33 hours after the event (top view) where one can see the re-covering of the different trajectories.

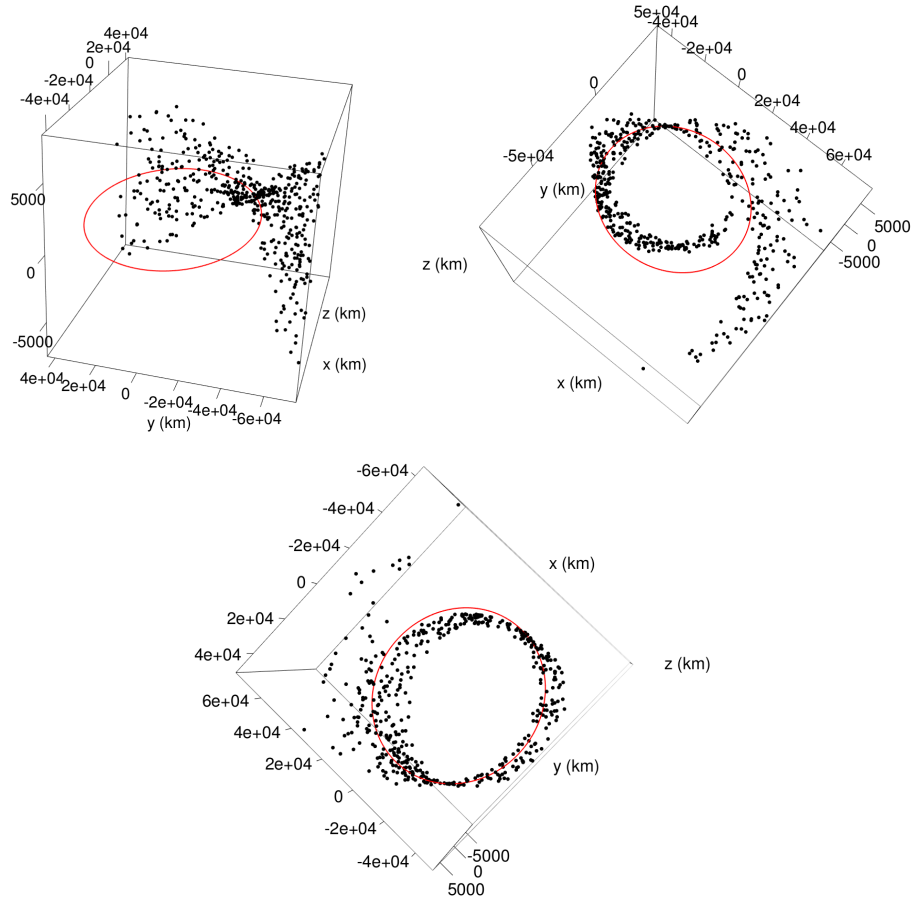


Figure 12: Top/left: shape of the cloud 12 hours after the explosion. Top/right: shape of the cloud (top view) 27 hours after the explosion. Bottom: shape of the space debris cloud (top view) after 33 hours of simulation. In the three cases, the red orbit represents the parent satellite evolution during the simulation if the breakup does not occur. Approximately 33 hours are necessary to populate the trajectory of the parent body because of the differences in orbital period induced by the explosion.

### *4.3. Influence of the location of the fragmentation along the orbit on the results of $G$ -function*

The value of the  $G$ -function that is estimated at a given epoch and for a given radius does depend upon the location of the breakup along the parent body's orbit. This dependence is stud-

ied in that section.

Three study cases are compared here. The parent body's orbit remains the same for each of the three cases, and namely a Molniya-like trajectory (Table 2, line 4) to clearly emphasise the role played by the eccentricity. The choice of an orbit with a high eccentricity is also motivated by the important velocity differences existing along this type of trajectory. The three test cases are defined by setting the mean anomaly equal to  $0^\circ$ ,  $90^\circ$  and  $180^\circ$  for cases 1, 2 and 3 respectively. The velocity increment distribution is chosen to correspond to the "Molniya realistic case" (maximum  $\Delta V$  equal to  $450 \text{ m.s}^{-1}$ ) and then depends on the initial velocity of the parent body at the epoch of the event. So before applying the distribution to the parent satellite, we set the upper bound of this distribution equal to 5% of the parent body velocity for case 1 and to 18% of the parent satellite velocity for cases 2 and 3. The orbits are propagated over 2 days, accounting only for the long periodic terms due to  $J_2$ , namely secular variations on the angles. Figure 13 shows the evolution with time of the  $G$ -function estimation for a ball radius (i.e.: a neighbourhood) of 210 km around a piece of space debris within the cloud. For each of the three study cases we chose to show only the results obtained for a radius of 210 km because the most important variations (see below) are visible in this neighbourhood.

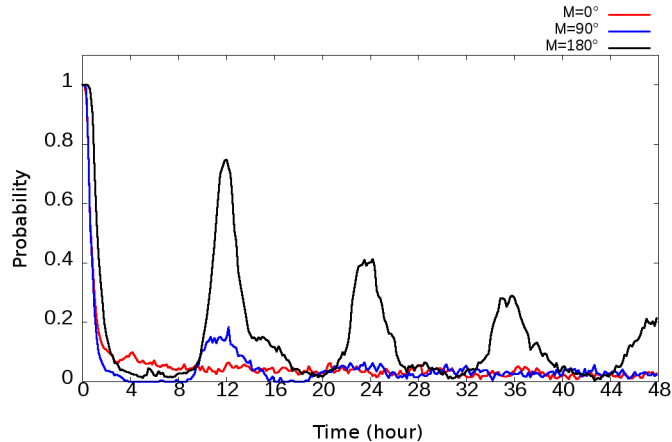


Figure 13: Probability of finding a neighbour in a radius of 210 km around a piece of space debris within the cloud, after the explosion, defined as realistic, of a satellite evolving on a Molniya-like orbit. The red, blue and black curves stand respectively for the cases where the mean anomaly at the epoch of the event is set equal to  $0^\circ$ ,  $90^\circ$  and  $180^\circ$ .

First of all, the initial eccentricity of this type of orbit ( $\approx 0.72$ ) induces variations in the evolution of the  $G$ -function with time. These oscillations are especially visible for  $M = 90^\circ$  and  $M = 180^\circ$  and occur every 6 hours approximately after the occurrence of the fragmentation, at least during the first day of simulation. Based on Figure 13, the probability is pretty high every 12 hours meaning that the objects within the cloud tend to get closer to each other. These changes in the  $G$ -function occur at the same moments after the explosion, independently from the initial location of the parent body along its orbit at the epoch of the event. Following this observation and knowing that the orbital period of an object evolving on a Molniya type of trajectory is around 12 hours, it can be deduced that, even if perigee and apogee crossings have an influence on the space debris cloud distribution because of the velocity changes, the variations are due to passages through special points of the trajectory. These locations are the “*pinch points*” [16] and correspond to the position of the orbit where the event occurred and its opposite.

More specifically, two features can be observed when the fragmentation occurs at the orbit’s perigee ( $M = 0^\circ$ , red curve). First, the probability of finding a neighbour is the smallest. Second, the

probability tends to stabilise relatively quickly (around 16 hours, a bit more than an orbital revolution) ; we interpret this stabilization as a total spreading of the cloud along the parent body’s orbit. An explosion occurring at the apogee of the trajectory (black curve) leads to the most visible increase of the probability around 12 hours and then 24 hours after the breakup; the same observation is even made for the case where  $M = 90^\circ$  (blue curve). Here, the stabilization of the probability of finding a neighbour occurs around 28 hours in the case of a breakup where  $M = 90^\circ$ , and, for an explosion occurring at the orbit’s apogee, the probability is not stabilised yet at the end of the simulation (2 days after the event).

Moreover, it is worth noting that the probability of finding a neighbour, and then the space debris density, is naturally greater when the breakup occurs at the apogee of the trajectory because the velocity of a payload is naturally smaller at that location. This explains the amplitude differences observed on Figure 13 and it also means that the collision probability between a fragment of the cloud and an outside object is greater for that breakup configuration.

As a conclusion, the location of the parent body along its orbit plays an important role for the spatial distribution variations of the cloud, and in particular on the spreading time of the fragments along the parent satellite trajectory, specifically in the case of a highly eccentric orbit as the Molniya type.

## 5. Conclusions and prospects

A new approach to estimate the spatial distribution of a space debris cloud generated by a fragmentation in orbit has been presented: the  $G$ -function based on point processes theory initially used in lots of others study fields (forestry, ecology, ...). It mainly uses the distances between objects of the studied population to get the probability of finding a neighbour in a given “perimeter” around a point (i.e. a fragment). Before the estimation, a so-called *observation window* has to be defined, including all the points belonging to the point process without creating gaps, as the distance between a particle and the window’s border is the second main characteristic to consider for the estimate. The observation window evolves through time with the shape of the cloud and is defined based on the spherical coordinates

of the extreme objects of the population. The behaviour of the  $G$ -function has been analysed when applied to the particular problem of studying the distribution of space debris, by carrying out some changes in the parameters of the simulation.

The influence of (i) the typical (maximum) value of  $\Delta V$ , (ii) the kind of orbit of the parent satellite, and **(iii) the location of the breakup along the orbit (i.e. position of the parent body on its orbit)** have been discussed. The parameters that induced the greatest differences in the evolution of the  $G$ -function are the maximum value of  $\Delta V$  (fragments are closer when this maximum value is small and reversely) and the orbit's type of the parent body (high eccentricities generate "periodic" variations on the orbital period). **Nevertheless, for strongly eccentric orbits, such as the one of a Molniya system, the location of the breakup has also a great influence on the cloud distribution because of the important velocity variations along this type of orbit.**

**Only the effects of the geopotential term (due to  $J_2$ ) are considered here** ; further analyses shall be carried out with the consideration of other perturbations (such as atmospheric drag) and the addition of space debris characteristics (as the direction of their velocity vector) in order to get closer to the definition of a collision probability instead of a probability of finding a neighbour in a given radius around a piece of space debris. On another hand, it will be interesting to check the influence of the size of the fragments on the distribution of the cloud. It should be interesting to consider the evolution of the  $G$ -function for a population of small pieces of space debris (less than 10 cm in diameter) in order to check the possible deviations with the population of fragments with a diameter greater or equal to 10 cm.

**Finally, the study of the existence of a path between the estimation of the  $G$ -function and the one of the spatial density should be carried out.** Based on the expression derived by [18], the spatial object density in a particular cell belonging to a discretised volume can be determined with two quantities: the cell volume and the resident probability related to that cell. An analogy can be made between that method and the use of the  $G$ -function ; the statistic presented in this paper can be estimated in each cell of a discretised observation window to get a spatial object density estimation with the equation described in [18] (p 64). In that case, the cell volume is determined from the discretised observation window and the resident probability is replaced by the estimation of the  $G$ -function in the cell. This method seems promising and will be

studied deeper in a future work.

## 6. Acknowledgements

We are very grateful to Carmen Pardini and Luciano Anselmo for providing the cartesian coordinates of the space debris generated by the Fengyun-1C fragmentation. This work is co-financed by Université de Lille and the Centre National d'Etudes Spatiales (CNES).

## References

- [1] C. Pardini and L. Anselmo. Physical properties and long-term evolution of the debris clouds produced by two catastrophic collisions in earth orbit. *Advances in Space Research*, 48:557–569, 2011.
- [2] C. Pardini and L. Anselmo. Evolution of the debris cloud generated by the fengyun-1c fragmentation event. C. Pardini and L. Anselmo in the 20th International Symposium on Space Flight Dynamics (ISSFD), Annapolis, 24-28 Sept 2007.
- [3] C. Pardini and L. Anselmo. Assessment of the consequences of the fengyun-1c breakup in low earth orbit. *Advances in Space Research*, 44:545–557, 2009.
- [4] C. Pardini and L. Anselmo. Revisiting the collision risk with cataloged objects for the iridium and cosmo-skymed satellite constellations. *Acta Astronautica*, 134:23–32, 2017.
- [5] N.L. Johnson, E. Stansbery, J.C. Liou, M. Horstman, C. Stokely, and D. Whitlock. The characteristics and consequences of the breakup of the fengyun-1c spacecraft. *Acta Astronautica*, 63:128–135, 2008.
- [6] J.C. Liou and N.L. Johnson. Characterization of the catalogued fengyun-1c fragments and their long-term effect on the leo environment. *Advances in Space Research*, 43:1407–1415, 2009.
- [7] L. Anselmo and C. Pardini. Long-term dynamical evolution of high area-to-mass ratio debris released into high earth orbits. *Acta Astronautica*, 67:204–216, 2010.
- [8] J. Illian, A. Penttinen, H. Stoyan, and D. Stoyan. *Statistical Analysis and Modelling of Spatial Point Patterns*. John Wiley and Sons, 2008.

- [9] A.J. Baddeley. Spatial sampling and censoring. In O.E. Barndorff-Nielsen, W.S. Kendall, and M.N.M. van Lieshout, editors, *Stochastic Geometry : Likelihood and Computation*, volume 80 of *Monographs on Statistics and Applied Probability*, pages 37–78. Chapman and Hall, London, England, 1999.
- [10] D. Stoyan. On estimators of the nearest neighbour distance distribution function for stationary point processes. *Metrika*, 64:139–150, 2006.
- [11] J. Moller and R.P. Waagepetersen. *Statistical Inference and Simulation for Spatial Point Processes*. Chapman and Hall/CRC, 2004.
- [12] A.J. Baddeley, E. Rubak, and R. Turner. *Spatial Point Patterns - Methodology and Applications with R*. Taylor and Francis Group, 2016.
- [13] M.N.M. Van Lieshout and A.J. Baddeley. A nonparametric measure of spatial interaction in point patterns. *Statistica Neerlandica*, 50:344–361, 1996.
- [14] F. Deleflie, D. Coulot, R. Descosta, A. Fernier, and P. Richard. First attempt of orbit determination of slr satellites and space debris using genetic algorithms. 6th European Conference on Space Debris, Darmstadt/Germany, 22-25 April 2013.
- [15] S. Casotto. The mapping of Kaula’s solution into the orbital reference frame. *Celestial Mechanics and Dynamical Astronomy*, 55(3):223–241, 1993. DOI: 10.1007/BF00692511.
- [16] R. Jehn. Dispersion of debris clouds from in-orbit fragmentation events. *ESA Journal*, 15:63–77, 1991.
- [17] J. Ashenberg. Formulas for the phase characteristics in the problem of low-earth-orbital debris. *Journal of Spacecraft and Rockets*, 31(6):1044–1049, 1994.
- [18] H. Klinkrad. *Space Debris - Models and Risk Analysis*. Praxis Publishing Ltd, Chicester, UK, 2006.